Chapter 8
Shear Thickening Fluid-Based Protective Structures Against High Velocity Impacts

Neelanchali Asija Bhalla

8.1 Introduction

Shear thickening fluid (STF) is an important class of non-Newtonian fluids, which exhibit transition from low viscosity to high viscosity under shear forces. The shear thickening phenomenon is reversible, making the STF revert to the initial low viscosity state upon the removal of applied shear [1]. Due to this remarkable feature, STF is extensively used in vibration damping systems [2–4], hip protection pads [5], and anti-impact applications [6–9]. In the last two decades, STF has been integrated into personal protection equipment to develop liquid body armor. In this regard, advanced protective textiles are treated with STF and efficiently used against various threats such as knives, spikes, and projectiles [10–12]. Although there is an extensive literature available on the low strain rate response of STF [13–15], there is a limited literature on STF characterization under high strain rate conditions. In this field, initial studies were conducted by Lim et al. [16] using split Hopkinson pressure bar (SHPB) technique for high strain rate characterization of STF. Lim et al. [17] reported the phenomenological modeling of the SHPB results to predict the mechanical response of STF under dynamic squeeze flow loading conditions. Thereafter, Asija et al. [18, 19] investigated the effect of particle size on the low and high strain rate behavior of STF, as well as reporting the mechanical characterization of STF under high strain rate dynamic compressive loading.

This chapter presents a review on the protective applications of STF under high velocity impact conditions. According to the outline of the chapter, the next section deals with the detailed description and classification of impacts in different

N. A. Bhalla (✉)
Mechanical Engineering Department, Bennett University, Greater Noida, Uttar Pradesh, India

Center for Nanosensors and Nanomedicine, Bennett University,
Greater Noida, Uttar Pradesh, India
e-mail: neelanchali.bhalla@bennett.edu.in

S. Gürgen (ed.), *Shear Thickening Fluid*,
https://doi.org/10.1007/978-3-031-25717-9_8

categories based upon impact velocities. The subsequent sections explain the various characterization techniques and test methods to determine the efficacy of STF at high strain rate conditions. Then, various STF impregnation techniques and their efficacy are discussed considering the protective applications. Furthermore, there is a discussion on the stability of STF under different environmental conditions such as high temperature, humidity, and ultraviolet (UV) radiation.

8.2 Classification of Impacts

The term "impact" can be defined as striking of an object forcibly onto another object. The degree of impact is measured in terms of severity of impact, i.e., damage occurred. Based upon the impact velocity, there are different categories: low velocity (large mass), intermediate velocity, high velocity, and hypervelocity impact as shown in Fig. 8.1.

It is important to categorize the impacts since there are drastic changes in the energy transfer phenomenon between the projectile and target. Furthermore, energy dissipation and damage mechanisms show variations by the change of impact velocity [20, 21]. Low velocity impacts occur at the velocities less than 10 m/s. Impacts occurring in the velocity range of 10–50 m/s are called intermediate velocity impacts, and impacts occurring at the velocity range of 50–1000 m/s are called high velocity impacts. Hypervelocity impacts are observed in the velocity range of 2–5 km/s [22].

8.3 Characterization of STF Under High Velocity Impacts

High velocity impact conditions produce high strain rate deformations in the materials. Figure 8.2 shows the classification of strain rates. For high strain rate levels, a special testing system namely split Hopkinson pressure bar (SHPB) test is used to characterize materials. In this testing procedure, strain rates from 10^2 to 10^4 s^{-1} are observed in the impact conditions. Figure 8.3 shows a typical SHPB testing system for high velocity impact conditions. As depicted in the figure, SHPB system

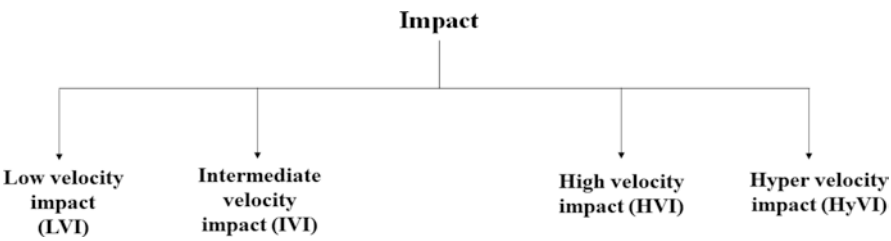

Fig. 8.1 Classification of impact based upon velocity

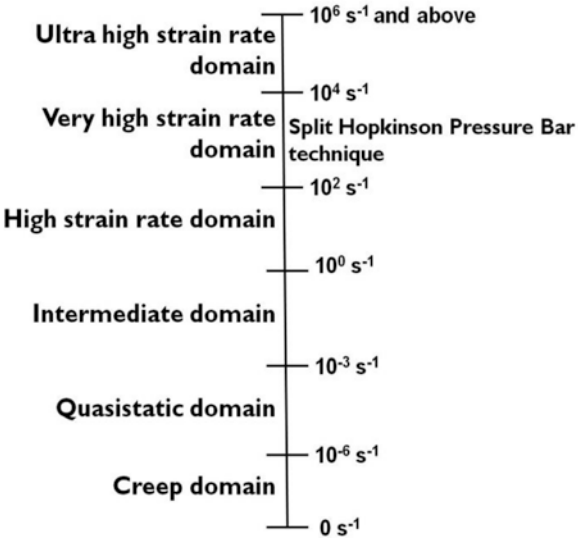

Fig. 8.2 Classification of strain rates

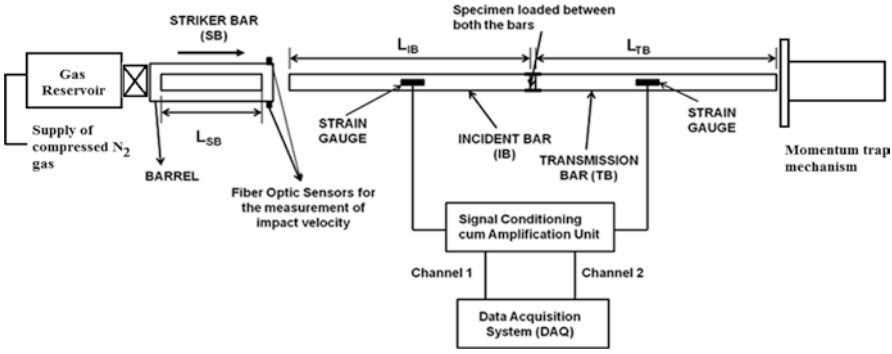

Fig. 8.3 Schematic illustration of an SHPB testing system

comprises three bars: striker bar, incident bar, and transmission bar. During the tests, striker bar is propelled through a long barrel under the pressure driven by a gas compressor. During striking on the incident bar, a part of the loading pulse is reflected back while the remaining part is carried through the transmission bar. The reflected and transmitted pulses are dependent on the mismatch of the acoustic impedance between the sample and bar. The term "acoustic impedance" is one of the materials properties that can be defined as the resistance by the medium in the propagation of longitudinal sound waves. Acoustic impedance depends upon the density and speed of sound through the material as given in Eq. (8.1).

$$Z = \rho \cdot C \tag{8.1}$$

where ρ is the density of the material, C is the speed of longitudinal waves in the material, and Z is the acoustic impedance of the material.

In the selection of bar material, the difference in the acoustic impedances of the sample and the bar is desired to be minimum to have a strong transmitted signal. For testing an STF in an SHPB system, the bar is generally made from AA6063 since the acoustic impedance of this alloy is quite close to that of STF. To have a successful SHPB test with an STF, the following conditions should be met.

1. The sample should be under a stable laminar flow.
2. The sample should be in a force equilibrium, i.e., the sum of the incident and reflected strains measured by the strain gauges should be equal to the transmitted strain.
3. A strong transmission signal should be obtained.

The satisfaction of above conditions contributes to the precise characterization of STF under high strain rate loadings. Prior to each test, a pulse shaper generally made of elastic rubber is placed at the impacting surface of the incident bar to increase the loading time since the pulse shaper deforms slower than the bar. This enables to have distinctive incident and reflected pulses while obtaining a near trapezoidal loading pulse (ε_i). The reflected and transmitted pulses are denoted by ε_r and ε_t, respectively. The magnitude of these pulses (ε_i, ε_r, and ε_t) is measured with strain gauges attached at the center of each bar. The specimen stress and strain are determined by using the SHPB equations, Eqs. (8.2, 8.3 and 8.4) given below;

$$\text{Compressional strain rate}: \ \dot{\varepsilon}s(t) = \left(\frac{2C_0}{Ls}\right)\varepsilon_r(t) \tag{8.2}$$

$$\text{Average strain}: \varepsilon s(t) = \pm\left(\frac{2C_0}{Ls}\right)\int_0^t \varepsilon_r(t)dt \tag{8.3}$$

$$\text{Average stress}: \sigma(t) = \pm E\frac{A_B}{A_S}\varepsilon t(t) \tag{8.4}$$

where, Co is the elastic wave velocity in the bars, Ls is the length of the sample, A_B is the cross-sectional area of the bar, A_S is the cross-sectional area of the sample, t is the duration, and E is the modulus of elasticity of the bar material.

The following assumptions are made in the relationships regarding the SHPB testing [23–25].

- Frictional and radial inertial effects are negligible.
- Wave propagation is considered by the one-dimensional wave theory with negligible wave dispersion.
- States of stress and strain are homogeneous in the sample.
- Sample is perfectly in contact with the bars during the impact.

Table 8.1 Experimental parameters in a typical SHPB system

Parameter	Value
Length of barrel	2000 mm
Material of bars	AA6063
Length of incident and transmission bar	1200 mm
Length of striker bar	85 mm
Diameter of incident and transmission bar	15.5 mm
Elastic modulus of bar material	68.9 GPa
Density of bar material	2.7 g/cm^3
Speed of sound in bar	5052 m/s
Thickness of sample	0.35 mm
Diameter of sample	15.5 mm

Table 8.1 shows the experimental parameters for a typical SHPB system. The gap size between the incident and transmission bars corresponds to the thickness of sample. However, STF is a fluidic sample and, therefore, this size is obtained by the application of Kuzma's dynamic squeeze flow model as given in Eq. (8.5) [16, 26].

$$F = \frac{\pi R^4}{4}\left[\frac{3\rho}{5h}\left(\ddot{U}_1 - \ddot{U}_2\right) + \frac{15\rho}{14h^2}\left(\dot{U}_1 - \dot{U}_2\right)^2 + \frac{6\mu}{\mathrm{h}^3}\left(\dot{U}_1 - \dot{U}_2\right)\right] \tag{8.5}$$

where,

F is the total force applied to the sample.
h is the instantaneous thickness of the sample (Hs (1-ε)).
Hs is the thickness of the sample.
ε is the strain in the sample.
μ is the viscosity.
ρ is the density of the sample.
$\left(\ddot{U}_1 - \ddot{U}_2\right)$ is the gap closing acceleration between the bars.
$\left(\dot{U}_1 - \dot{U}_2\right)$ is the gap closing speed between the bars.

The terms "gap closing speed" and "gap closing acceleration" are illustrated in Fig. 8.4. As given in the schematic, U_1 is the displacement of the incident bar, U_2 is the displacement of the transmission bar, and h is the instantaneous thickness of the fluid sample. Since the thickness of the fluid sample varies continuously during the loading and unloading period, instantaneous sample thickness is considered as a function of time while depending on the strain. From Fig. 8.4, it is clear that the fluid sample initially undergoes an axial compression during the loading phase of the cycle when the incident bar moves axially. Thereafter, the fluid sample undergoes a squeezing and radially expanding phase between the bars.

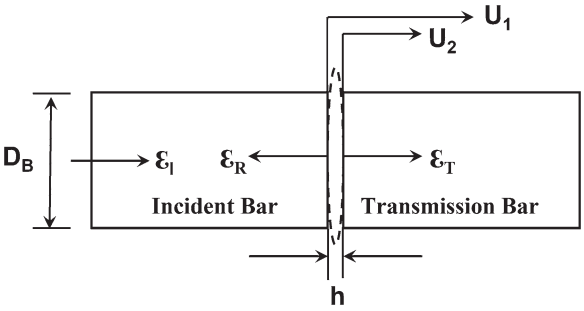

Fig. 8.4 Squeezing of the fluid sample under dynamic compressive loading

To determine the appropriate thickness of the fluid sample, the squeeze flow model is validated by using a standard fluid with a known viscosity. The viscous force in Eq. (8.5) can be written as in Eq. (8.6).

$$F_{\text{viscous}} = \frac{\pi R^4}{4}\left[\frac{6\mu}{h^3}\left(\dot{U}_1 - \dot{U}_2\right)\right] \tag{8.6}$$

By rearranging the terms in Eq. (8.6), the viscous force is obtained in Eq. (8.7).

$$\left(\frac{2h^3}{3\pi R^4}\right)F_{\text{viscous}} = \mu\left(\dot{U}_1 - \dot{U}_2\right) \tag{8.7}$$

All the terms in Eq. (8.7) are known except for the viscosity, which is the slope for the given relationship. Asija et al. [18] investigated a standard viscosity oil, N4000, to validate the sample thickness. The density and viscosity of the oil were known at different temperatures in accordance with ISO 17025 as provided by the manufacturer. To determine the sample thickness experimentally, the gap width between the incident and transmission bars was maintained at the desired value using a feeler gauge. The gap width was varied from 0.30 to 0.45 mm while firing each shot by keeping the pressure of the compressed gas constant at 0.2 bar. All the forces; the transient inertial force, bulk inertial force, viscous force, and experimental force were calculated for each shot. Figure 8.5 shows the relationship between the viscous force and gap closing speed based on the data obtained from the SHPB tests. The slope of the curve was calculated to determine the viscosity for different gap widths. The viscosities experimentally obtained from the graphs were compared with the viscosity given in the manufacturer's specifications. Based on the results, the experimental viscosity obtained for the gap width of 0.35 mm was the closest one to the viscosity given in the product sheet. Hence, sample thickness for SHPB testing was determined based on this procedure. Since the sample was a fluid, all the cross-sectional area of the bars was covered with the sample and, therefore, the diameter of the sample was considered as the diameter of the bars.

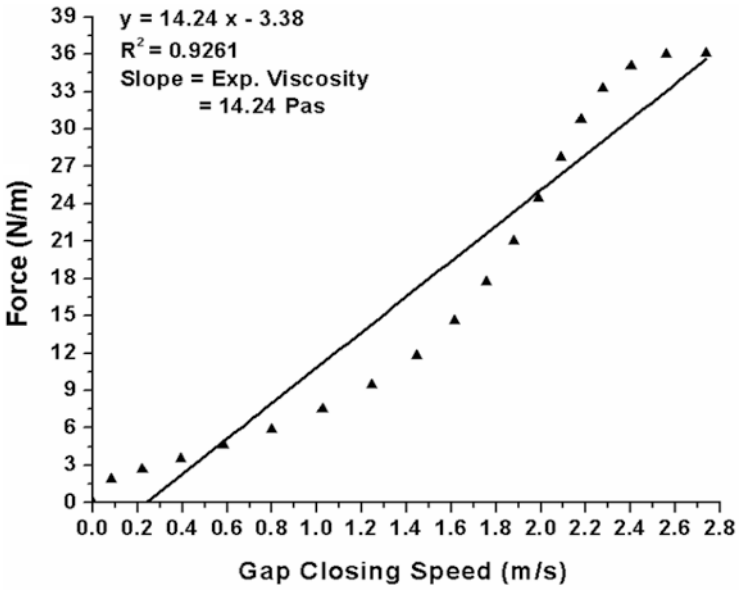

Fig. 8.5 Viscous force vs gap-closing speed for the standard oil N4000

After deciding on the dimensions of the sample, there is a list of steps followed to carry out the testing. The first step is calibration for ensuring reliable results. Calibration is done for two key points: (1) force calibration and (2) pressure-velocity calibration. In the force calibration procedure, the test is run without a sample between the incident and transmission bars. Since there is no specimen, there is no acoustic mismatch at the interface of the bars, thereby resulting in a complete passing of the stress pulse from the incident bar to the transmission bar without generating any reflected pulse. If the force measured by the strain gauge mounted on the incident bar equals to the force measured by the strain gauge mounted on the transmission bar upon running the test, stress states in the both bars become identical, which means that the system is perfectly aligned and ready for testing. On the other hand, the relationship between the impact velocity of the striker bar and the gas pressure of the gun is obtained in the pressure-velocity calibration. The impact velocity is measured with the help of fiber optic sensors, which are mounted at the specific locations with certain distances from each other.

A high-speed counter module equipped with programmable logic controller (PLC) is used to determine the time period between the sensors as the striker bar passes through the beam of the sensors before hitting the incident bar. This helps to compute the impact velocity of the striker bar. Figure 8.6 shows the schematic illustration of an impact velocity measurement system in the SHPB system.

After completing both calibration procedures, STF is applied at the interface of the incident and transmission bars by adjusting the gap width by the help of a feeler gauge. After applying the sample, the striker bar is fired by releasing the compressed

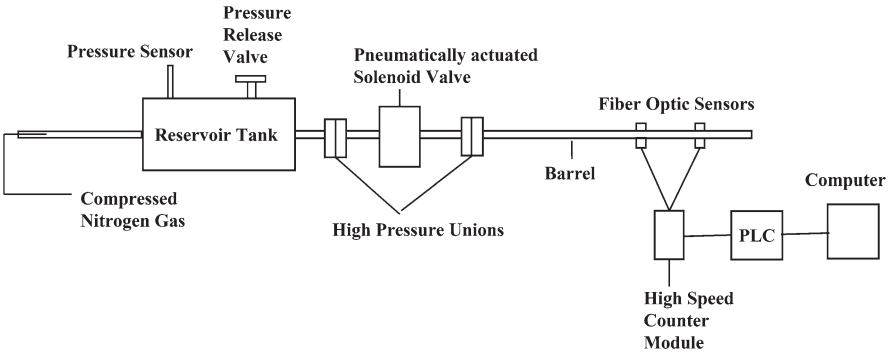

Fig. 8.6 Impact velocity measurement system in the SHPB system [18]. Reprinted by permission from Elsevier

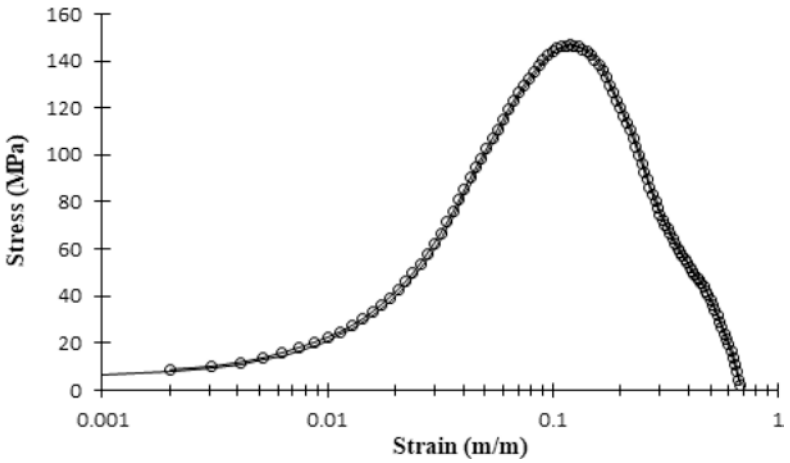

Fig. 8.7 Stress vs strain curve for an STF

gas. It is important to note that the test should be started immediately after the sample application to avoid STF leakage between the bars. Because STF is a viscous fluid, it shows loading and unloading cycles under dynamic compressive loading. For STF characterization on SHPB apparatus, one of the outputs is the stress and strain relationship during the impact. A typical graph of the stress vs strain curve for an STF is given in Fig. 8.7. It is clearly seen that there is a sharp increase in the stress beyond the critical strain. The stress induced in the sample is a measure of the capability to resist the deformation. Hence, higher stress magnitudes exhibit higher resistance to dynamic compressive impact. Since the stress is calculated from the magnitude of transmitted strain as given in Eq. (8.4), it is desirable to have a strong transmission signal in the SHPB testing. Another output is the relationship between strain rate and strain in the SHPB testing. Figure 8.8 shows a typical strain rate vs strain curve for an STF obtained from the SHPB testing. Similar to the

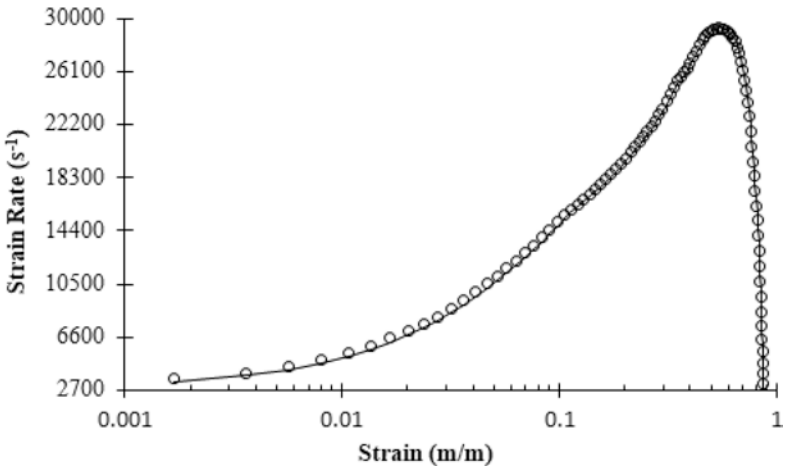

Fig. 8.8 Strain rate vs strain curve for an STF

relationship between stress and strain, strain rate curve increases beyond the critical point. The strain rate can be calculated by using Eq. (8.2) and requires the magnitude of the reflected pulse. The strain rate is a measure of loading rate for the sample, which implies how fast the sample is loaded to the peak value of the stress. To sum up, it is obvious that there is an increase in both stress and strain rate beyond a critical strain, which point out the onset of shear thickening phenomenon under dynamic compressive loading. This is completely analogous with the steady shear testing conducted with a rheometer, wherein the critical shear rate triggers the onset of the shear thickening behavior.

Characteristic transition time (CTT) is defined as the time required by STF to make the transition from the low viscosity state to high viscosity state. CTT is a characteristic feature of STF and provides more about the STF in addition to the stress and strain curves. CTT is influenced by all the parameters, which play a crucial role in the rheological behavior of STF such as particle size, particle size distribution, particle shape, particle hardness, and liquid medium. CTT is an important metric for the STF-included structures under dynamic loading. Generally, the CTT of an STF varies on a scale from microseconds to milliseconds. Technically, it is not possible to determine the CTT by using a commercial rheometer due to the operation timescales of milliseconds. For this reason, CTT is obtained from the SHPB testing. Figure 8.9 shows the compressive acceleration curve of an STF indicating the CTT on the graph. In the SHPB testing, the onset of shear thickening leads to the deceleration of the bars during the loading part of the stress cycle. The compressive acceleration is computed by taking the time derivative of the gap-closing speed at each instant and then subsequently plotting it with respect to time. The instance of the first deceleration in the plot, as seen in Fig. 8.9, indicates the onset of shear thickening phenomenon while providing the CTT of the STF. This information can only be deduced from the SHPB testing.

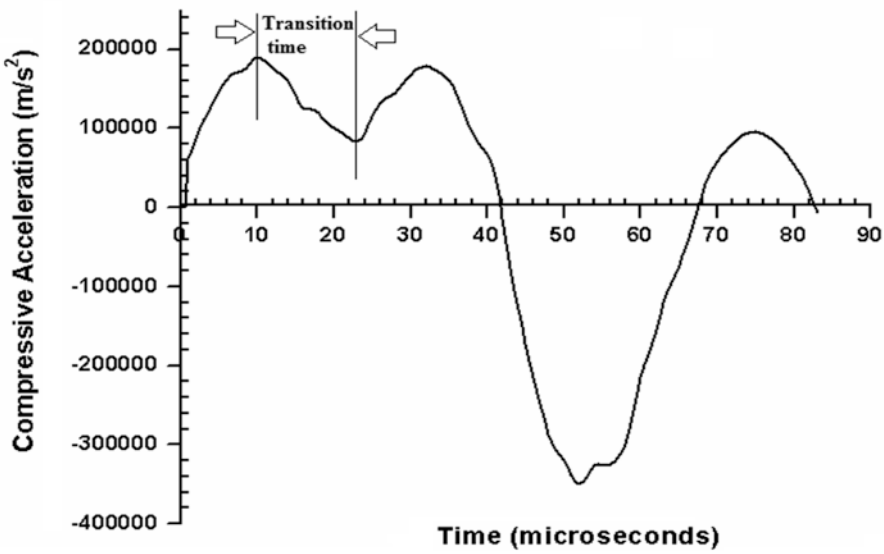

Fig. 8.9 CTT of an STF in the compressive acceleration curve

8.4 STF Applications in High Velocity Impact Resistant Protective Structures

As given in the previous sections, high velocity impact falls in the category of impact velocity range from 50 to 1000 m/s. In a high velocity impact event, it is very crucial to determine the strain rates and the CTT of the STF. Without knowing these parameters, it is highly difficult to ascertain the efficacy of STF under dynamic loading conditions.

Packaging technique of STF in protective structures is very crucial as it dictates the deformation and failure kinetics under high velocity impacts. According to the literature, STF-based protective structures can be produced in two different ways. In the first method, advanced engineering textiles are impregnated with STF by soaking the fabrics in a diluted STF pool. Then, the fabrics are rested to remove the excessive liquid and diluting agent. In the other method, STF is packed as a bulk liquid in a container and used as a liquid component in the structures. The use of STF in personal protection systems requires the development of special design to facilitate the incorporation of STF in different ways [27]. In the STF-integrated structures, it is imperative that the entire system is leak proof to prevent any leakage of STF in the impact events, thereby sustaining the anti-impact properties of the complete system. The structures can be modular in such a way that they may show the STF leakage only at a localized impacted area while preserving the efficacy of the remaining structure. Wisniewski et al. [27] proposed such kind of structural design including STF. It was observed that the STF-containing modules, which

were made of ballistic fabrics, performed better against high velocity impacts in comparison to the other designs including STF-impregnated fabrics.

There are several studies discussing the high velocity impact behavior of STF-included structures. De Goede et al. [28] reported the capability of complex non-Newtonian fluids to stop or retard the projectiles under high velocity impacts. It was stated that impact resistance can be attributed to the viscoelastic nature of the fluids rather than the shear thickening or shear thinning behavior. Hence, for the fabrication of liquid body armors, the focus shifted to use of polymeric viscoelastic fluids for an enhanced ballistic resistance. However, it was also observed that the anti-impact performance was higher with shear thickening suspensions in comparison to the other polymeric fluids. Kim et al. [29] studied the impact resistance of two different ballistic fabrics after impregnating with STF. The fabrics were also coated with a multi-purpose adhesive. Yarn pull-out tests and high velocity ballistic tests were conducted to characterize the fabrics. It was observed that STF impregnation provides no change in the flexibility of the ballistic fabrics; however, the yarn pull-out force as well as the energy absorption per unit areal density shows higher levels for adhesive-coated fabrics. Wei et al. [30] studied the effect of silica morphology on the stab resistance of STF-impregnated textile composites under dynamic impact conditions. Spherical silica-based STF was found to perform better as compared to the irregular-shaped silica STF in terms of induced stress and post-shear thickening viscosity under impact. Liu et al. [31] investigated the ballistic impact performance of multi-phase STF-impregnated high-performance fabrics against the titanium projectiles with the impact velocity of 250 m/s. Three different multi-phase STFs were fabricated by including graphene oxide (GO), carbon nanotubes (CNT), and a mixture of both in the suspensions. It was observed that multi-phase STFs exhibit enhanced yarn pull-out forces, lower value of critical shear rates, and post-shear thickening viscosity as compared to the single-phase STF. Moreover, the GO-based STF exhibited the highest energy absorption capability under high velocity impact testing among the investigated suspensions. With an objective to develop a low cost and biocompatible armor, Cho et al. [32] designed a bulletproof composite comprising composite panels and cornstarch-based STF. Contrary to the common STF applications, the composite panels were not impregnated with STF. In the target design, STF was kept in a sealed plastic bag, which was further encapsulated in a plastic container. It was observed that the normalized perforated area of the ballistic composite decreased with the increase in the thickness of STF layers as compared to the neat composite layers.

In addition to the impact resistance performance, there are various works dealing with the durability of STF in anti-impact structures. Since the protective structures are mainly used in open to atmospheric conditions, some key factors such as temperature, humidity, and UV radiation gain importance. Soutrenon et al. [33] studied the effect of processing methods and storage on the efficacy of STF. The efficacy was studied in terms of the change in critical shear rate and post-shear thickening viscosity. In their study, STF was prepared using hand mixing technique followed by sonication in an ultrasonic bath, jar rolling, and simply hand mixing the suspension followed by a vacuum degassing step. According to the results, increasing the

processing duration in sonication leads to a marginal increase in the viscosity at low shear rates while increasing the magnitude of shear thickening behavior, i.e., growing the peak viscosity. On the other hand, critical shear rate is significantly reduced by prolonging the sonication process. In order to investigate the storage conditions, STF samples were kept in different conditions as given below:

1. In a chamber with 22% relative humidity at ambient temperature for 45 days
2. In a chamber with 100% relative humidity at ambient temperature for 45 days
3. In a chamber with nitrogen gas at ambient temperature for 15 days
4. In a chamber at −24° C for 45 days
5. In a chamber at ambient temperature by encapsulating between two silicone layers for 15 days

It was observed that glycols are extremely hydrophilic in nature. They have high tendency to absorb moisture from the environment, thereby contaminating STF and causing deterioration in the shear thickening properties. As the molecular weight of glycols increases, the tendency to absorb moisture decreases. The STF at −24° C could preserve the shear thickening properties for the entire test duration. Since these conditions can only be found in laboratory, the efficacy of STF was checked in an encapsulation also. It was found that encapsulating STF in silicone tends to keep the shear thickening properties. From these results, it can be stated that STF encapsulation technique ensures to avoid any contact with air or contaminants in the ambient in order to have a prolonged service life of STF used in harsh conditions. Żurowski et al. [34] explored the influence of UV radiation on the shear thickening behavior. The synthesized STF samples were subjected to accelerated aging conditions with UV exposure for a total time period of 167 h, which corresponds to a natural aging period of 15.5 weeks. It was observed that prolonged exposure to UV radiation changes the oligomer structure to be degraded, thereby converting the liquid texture of STF into a solid phase. Consequently, the shear thickening behavior is completely lost. From these studies, it can be concluded that STF is susceptible to environmental conditions and, therefore, shear thickening properties are heavily affected by the ambient. In general, protective structures are used in harsh conditions including extremely low or high temperatures, humidity, and UV exposure; therefore, STF included protective systems should be designed taking all these issues into consideration.

8.5 Conclusions

There is a vast literature available on the rheological characterization of STF under steady and dynamic shear conditions. Researchers have also studied the anti-impact performance of advanced textiles with STF treatments; however, there is a limited literature discussing the efficiency of STF under high velocity impacts. For the STF usage against high velocity impacts, it is imperative to characterize the STF under high shear rates. The SHPB testing is a good way to do so. The information

delivered from the rheological tests are sometimes insufficient to ascertain the STF efficacy under high strain rate conditions. Moreover, it is also necessary to conduct investigations on the durability of STF in addition to the high strain rate characterizations. These studies help to determine the effect of environmental factors on the shear thickening behavior. As STF essentially comprises oligomers as the carrier fluid, its viscosity, and eventually shear thickening behavior, is drastically affected by the change in temperature. Similar to the temperature effect, humidity and UV exposure directly influence the microstructural properties of STF and thereby alter the shear thickening characteristics in the suspension. Because protective structures are mostly used in open to atmospheric conditions, they are subjected to various harsh conditions. For this reason, it is important that STF-based protective systems should be designed by considering the environmental effects on the shear thickening mechanism. Furthermore, STF should be isolated from the environmental exposures to avoid degradation in the shear thickening behavior.

References

1. S. Gürgen, M.C. Kuşhan, W. Li, The effect of carbide particle additives on rheology of shear thickening fluids. Korea Aust Rheol J. **28**(2), 121–128 (2016)
2. C. Fischer, A. Bennani, V. Michaud, E. Jacquelin, J.A.E. Månson, Structural damping of model sandwich structures using tailored shear thickening fluid compositions. Smart Mater. Struct. **19**(3), 035017 (2010)
3. C. Fischer, S.A. Braun, P.E. Bourban, V. Michaud, C.J.G. Plummer, J.A.E. Månson, Dynamic properties of sandwich structures with integrated shear-thickening fluids. Smart Mater. Struct. **15**(5), 1467 (2006)
4. S. Gürgen, M.A. Sofuoğlu, Experimental investigation on vibration characteristics of shear thickening fluid filled CFRP tubes. Compos. Struct. **226**, 111236 (2019)
5. S.N. Robinovitch, W.C. Hayes, T.A. McMahon, Energy-shunting hip padding system attenuates femoral impact force in a simulated fall. J. Biomech. Eng **117**, 409–413 (1995) http://biomechanical.asmedigitalcollection.asme.org/
6. M.J. Decker, C.J. Halbach, C.H. Nam, N.J. Wagner, E.D. Wetzel, Stab resistance of shear thickening fluid (STF)-treated fabrics. Compos. Sci. Technol. **67**(3–4), 565–578 (2007)
7. S. Gürgen, M.C. Kuşhan, Improvement of spall liner performance with smart fluid applications. Thin-Walled Struct. **180**, 109854 (2022)
8. M.R. Sheikhi, S. Gürgen, Deceleration behavior of multi-layer cork composites intercalated with a non-Newtonian material. Arch. Civ. Mech. Eng **23**(1), 1–11 (2023)
9. V.B.C. Tan, T.E. Tay, W.K. Teo, Strengthening fabric Armour with silica colloidal suspensions. Int. J. Solids Struct. **42**(5–6), 1561–1576 (2005 Mar)
10. S. Gürgen, T. Yıldız, Stab resistance of smart polymer coated textiles reinforced with particle additives. Compos. Struct. **235**, 111812 (2020)
11. S. Gürgen, F.A.O. Fernandes, R.J.A. de Sousa, M.C. Kuşhan, Development of eco-friendly shock-absorbing Cork composites enhanced by a non-Newtonian fluid. Appl. Compos. Mater. **28**(1), 165–179 (2021)
12. D.P. Kalman, R.L. Merrill, N.J. Wagner, E.D. Wetzel, Effect of particle hardness on the penetration behavior of fabrics intercalated with dry particles and concentrated particle-fluid suspensions. ACS Appl. Mater. Interfaces **1**(11), 2602–2612 (2009)
13. S. Gürgen, M.C. Kuşhan, The effect of silicon carbide additives on the stab resistance of shear thickening fluid treated fabrics. Mech. Adv. Mater. Struct. **24**(16), 1381–1390 (2017)

14. S.R. Raghavan, S.A. Khan, Shear-thickening response of Fumed silica suspensions under steady and oscillatory shear. J. Colloid Interface Sci. **185**, 57 (1997)
15. H. Yang, J. Ruan, J. Zou, Q. Wu, Z. Zhou, Z. Zhou, Rheological responses of fumed silica suspensions under steady and oscillatory shear. Sci. China Technol. Sci **52**(4), 910–915 (2009 Apr)
16. A.S. Lim, S.L. Lopatnikov, J.W. Gillespie, Implementing the Split-Hopkinson pressure bar technique for shear thickening fluid evaluation. AIP Conf Proc **1027**, 689–691 (2008)
17. A.S. Lim, S.L. Lopatnikov, N.J. Wagner, J.W. Gillespie, Phenomenological modeling of the response of a dense colloidal suspension under dynamic squeezing flow. J. Nonnewton Fluid Mech **166**(12–13), 680–688 (2011 Jul)
18. N. Asija, H. Chouhan, S.A. Gebremeskel, N. Bhatnagar, High strain rate characterization of shear thickening fluids using Split Hopkinson pressure Bar technique. Int J Impact Eng **110**, 365–370 (2017a)
19. N. Asija, H. Chouhan, S.A. Gebremeskel, N. Bhatnagar, Influence of particle size on the low and high strain rate behavior of dense colloidal dispersions of nanosilica. J Nanopart Res. **19**(1), 3723 (2017b)
20. S. Gürgen, The influence of boundary condition on the impact behavior of high performance fabrics. Adv. Electron. Forum **28**, 47–54 (2018)
21. N.K. Naik, P. Shrirao, Composite structures under ballistic impact. Compos. Struct. **66**(1–4), 579–590 (2004 Oct)
22. S.N.A. Safri, M.T.H. Sultan, N. Yidris, F. Mustapha, Low velocity and high velocity impact test on composite materials-a review. Int. J. Eng. Sci **3**(9), 50–60 (2014) Available from: www.theijes.com
23. H. Kolsky, An Investigation of the Mechanical Properties of Materials at very High Rates of Loading. Proc. Phys. Soc. **62**, 676–699 (1949)
24. N.K. Naik, V. Ch, V.R. Kavala, Hybrid composites under high strain rate compressive loading. Mater. Sci. Eng. A **498**(1–2), 87–99 (2008)
25. S.C. Woo, T.W. Kim, High-strain-rate impact in Kevlar-woven composites and fracture analysis using acoustic emission. Compos. Part B Eng **60**, 125–136 (2014)
26. A.S. Lim, S.L. Lopatnikov, J.W. Gillespie, Development of the split-Hopkinson pressure bar technique for viscous fluid characterization. Polym. Test. **28**(8), 891–900 (2009)
27. W. Adam, P. Dawid, Z. Pawel, W. Lukasz, K. Joanna, Z. Dorota, et al., Optimization of material systems with shear thickening fluids, in *28th International Symposium on Ballistics*. Atlanta, GA, (2014), pp. 1–10
28. T.C. de Goede, K.G. de Bruin, D. Bonn, High-velocity impact of solid objects on Non-Newtonian Fluids. Sci Rep **9**(1), 1250 (2019)
29. Y.H. Kim, S.K. Sathish Kumar, Y. Park, H. Kwon, C.G. Kim, *High-Velocity Impact onto a High-Frictional Fabric Treated with Adhesive Spray Coating and Shear Thickening Fluid Impregnation*, vol 185 (Compos B Eng., 2020), p. 107742
30. R. Wei, B. Dong, F. Wang, J. Yang, Y. Jiang, W. Zhai, et al., Effects of silica morphology on the shear-thickening behavior of shear thickening fluids and stabbing resistance of fabric composites. J. Appl. Polym. Sci. **137**(24), 1–7 (2020)
31. L. Liu, M. Cai, X. Liu, Z. Zhao, W. Chen, Ballistic impact performance of multi-phase STF-impregnated Kevlar fabrics in aero-engine containment. Thin-Wall. Struct **157**(29), 107103 (2020). https://doi.org/10.1016/j.tws.2020.107103
32. H. Cho, J. Lee, S. Hong, S. Kim, Bulletproof performance of composite plate fabricated using shear thickening fluid and natural fiber paper. Appl. Sci. **10**(1), 88 (2020)
33. M. Soutrenon, V. Michaud, J.A.E. Manson, Influence of processing and storage on the shear thickening properties of highly concentrated monodisperse silica particles in polyethylene glycol. Appl. Rheol. **23**(5), 20–28 (2013)
34. R. Żurowski, M. Tryznowski, S. Gürgen, M. Szafran, A. Świderska, The influence of UV radiation aging on degradation of shear thickening fluids. Materials **15**(9), 3269 (2022)